Excited-state-absorption and upconversion studies of Nd^{3+}-doped single crystals $Y_3Al_5O_{12}$, $YLiF_4$, and $LaMgAl_{11}O_{19}$

Y. Guyot, H. Manaa, J. Y. Rivoire, and R. Moncorgé
Laboratoire de Physico-Chimie des Matériaux Luminescents, Université de Lyon I, URA 442 CNRS, 69622 Villeurbanne, France

N. Garnier, E. Descroix, M. Bon, and P. Laporte
Laboratoire du Traitement du signal et de l'Instrumentation, Université de St. Etienne, URA 842 CNRS, 42023 St. Etienne, France
(Received 10 May 1994; revised manuscript received 22 September 1994)

In this paper we derive expressions for the laser slope efficiency and the threshold absorbed pump power which explicitly include excited-state absorption in the pump as well as in the laser-emission-wavelength domains. They are applied to the case of the diode-pumped Nd^{3+}-doped laser systems and, along with expressions allowing the calculation of excited-state-absorption (ESA) cross sections within the framework of the Judd-Ofelt theory, they provide a theoretical framework for the second part in which we present both experimental measurements and theoretical calibrations and an analysis of excited-state-absorption spectra in the stimulated emission as well as in the pumping domains of Nd^{3+}-doped $Y_3Al_5O_{12}$, $YLiF_4$, and $LaMgAl_{11}O_{19}$ laser crystals. The results indicate that ESA in the infrared metastable state of Nd^{3+} in these materials is negligible at the main laser wavelengths but can be more significant if it takes place, following some energy-transfer induced-excitation process, in higher-lying excited states. The analysis of these ESA within the Judd-Ofelt formalism shows a general agreement better than 50% between the experimental data and the theoretical predictions. This is used to estimate the influence of ESA in the pumping domain on the laser performance of the materials. It is found that it contributes but that it does not significantly perturb this laser performance, and that this effect is much less than some upconversion energy transfers that limit the fluorescence excitation efficiencies and reduce the energy-storage capacities by the reduction of the effective fluorescence lifetimes of the laser metastable level.

I. INTRODUCTION

The study of excited-state-absorption (ESA) or multiphoton-sequential-absorption phenomena generally allows the completion of classical one-photon ground-state-absorption (GSA), ground-state-emission, and dynamical-fluorescence studies. ESA allows us to probe high-energy-lying excited states drowned in continua, which are difficult to distinguish or to which the GSA transition probability is too weak to be observed, and to know more about the relaxation dynamics of the short-lived excited states, such as in plasma.[1]

The determination of the ESA cross sections in the absorption and emission domains gives essential information about the operation mode and the performance of laser systems based on the transition-metal[2,3] and rare-earth ions emitting in the near-infrared spectral region. It is also very informative in the study of future laser systems, so-called up conversion and photon-avalanche systems, emitting in the visible range.[4–6] The excited-state absorption of the pumping light, and the multiphonon relaxations that follow, also could partly explain the thermal overloading processes observed at high pumping power in the laser rods when the operating regime changes from a stimulated (lasing) to a spontaneous-emission regime.[7]

No direct and quantitative study of ESA has been conducted so far in the case of the now well-known Nd^{3+}-doped laser crystals $Y_3Al_5O_{12}$ (YAG) and $YLiF_4$ (YLF), either because no one realized the importance of it, or because the experimental measurements it necessitates were not easy to perform. To our knowledge, the only works that explicitly treat the ESA were conducted in glassy materials.[8–10] In the case of crystals, we note a nondirect measurement of an ESA cross section in YAG:Nd^{3+} around 750 nm (Ref. 11) and an ESA spectrum in SrF_2:Nd^{3+} around 1.06 μm.[12]

Thus, one did not know the real influence of this phenomenon, so detrimental in the case of the transition-metal-ion laser systems,[2,3] on the laser performance of the Nd^{3+}-doped crystals and what perspectives it could offer. One also did not know to what extent the existing formalisms, such as the Judd-Ofelt theory,[13,14] associated with the Einstein reciprocity law between the absorption and stimulated-emission cross sections, were able to give an account of the intrinsic cross sections of the optical transitions involved.

By testing a number of theoretical and experimental methods on well-known laser systems such as YAG:Nd^{3+} and YLF:Nd^{3+}, as mentioned above, and by applying them to the less common and more complex $LaMgAl_{11}O_{19}$:Nd^{3+} (or LMA:Nd^{3+} or LNA) laser crystal,[15] we fill an important scientific vacancy. Moreover, by studying more carefully the relationships between the intrinsic spectroscopic properties of these materials (such as stimulated emission and ESA cross sections, inhomo-

geneous versus homogeneous line broadening, etc.) and their laser performance,[16,17] we are able to deduce some additional information about their optical quality and about the importance of eventual impurities. This can be useful to the crystal grower spending time and money to improve the fabrication processes.

The first part of this work is devoted to theoretical considerations concerning the effect of ESA on the laser performance and the Judd-Ofelt calibration or prediction of the ESA spectra. In the second part we first give the results of experimental and theoretical calibrations in units of cross sections of polarized ESA spectra that were previously reported in another article.[15] The ESA spectra were recorded in the main regions of infrared-stimulated emission around 1.06 and 1.32 μm of Nd^{3+}-doped $Y_3Al_5O_{12}$ (YAG), $YLiF_4$ (YLF), and $LaMgAl_{11}O_{19}$ (LMA) laser crystals. We then give for the same systems ESA data obtained in the blue and the red regions at wavelengths that can be important in the parametrization of the photon avalanche process, which was enlightened recently,[4-6] and also for the estimation of the importance of ESA in the case of broadband flash-lamp pumping. Finally, data are presented concerning the competitive effects of upconversion energy-transfer processes, in particular when the systems are pumped by lasers, Ti-sapphire or semiconductor diode lasers, around 800 nm.

II. THEORETICAL CONSIDERATIONS

A. Effect of ESA on laser performance

In this subsection, we are going to treat the effect of ESA in the wavelength domains of laser emission (a case already examined in the past[15]) and of optical pumping on the laser performance (threshold pump power and laser efficiency) of a four-level laser system (for the case of the Nd^{3+}-doped systems emitting around 1.06 μm).

We first consider a laser crystal of thickness d within a two-mirror symmetrical cavity with an output coupler of transmission T and we assume stationary conditions. Then we introduce a simple model with a ground state 0 and two excited states 1 and 2, in which we assume that all of the photons absorbed in the excited state 1 are lost for laser action, which is a pessimistic view of the problem, and that there is negligible ground-state absorption (GSA) at the laser wavelength, which is justified in the case of a four-level laser system. Of course, for a Nd^{3+}-doped laser system emitting around 1.06 mm, the levels 0, 1, and 2 stand for levels $^4I_{9/2}$, $^4F_{3/2}$, and one of the higher-lying excited states of the Nd^{3+} ion, respectively. σ_0^P and σ_1^P are the GSA and ESA cross sections at the pump wavelength; σ_1^L is the ESA cross section at the laser wavelength; σ_{em} is the stimulated emission cross section; W is the spontaneous emission rate; and τ is the fluorescence lifetime of level 1. With these parameters, we solve, for a longitudinal pumping, the following equations of evolution:

$$\frac{dI_p}{dz} = -(\sigma_0^p N_0 + \sigma_1^p N_1) I_p \ , \tag{1}$$

$$\frac{dI_L^{\pm}}{dz} = \pm(\sigma_{em} - \sigma_1^L) N_1 I_L^{\pm} \ , \tag{2}$$

$$\frac{dN_1}{dt} = \sigma_0^p N_0 I_p - (\sigma_{em} + \sigma_1^L) N_1 I_L - \sigma_1^p N_1 I_p - W N_1 \tag{3}$$

with $N \cong N_0 + N_1$ and $I_L = I_L^+ + I_L^-$. N is the total ion density, and I_L^+ and I_L^- are the counter-propagating laser intensities in the cavity.

Within this framework, the threshold absorbed pump power and the laser output power are given by the following expressions:

$$P_{abs}^{th} \cong \frac{G^{2r}-1}{2\sigma_1^p \tau} \frac{1-\Theta_0}{1-\Theta G^r} h\nu_p S \ , \tag{4}$$

$$P_{laser} = \rho_{diff}(P_{abs} - P_{abs}^{th}) \ , \tag{5}$$

$$\rho_{diff} \cong \frac{h\nu_L}{h\nu_p} \frac{T}{2} \frac{2\sigma_1^p}{\sigma_{em} + \sigma_1^L} \frac{1}{G^{2r}-1} \frac{1-\Theta G^{2r}}{1-\Theta_0} \ . \tag{6}$$

ρ_{diff} is the laser slope efficiency; $h\nu_p$ and $h\nu_L$ are the energies of the pump and laser photons; S is an average cross-section area of the pump and cavity modes within the laser crystal; Θ_0 and Θ are the transparencies of the crystal at the pump wavelength below and above laser threshold, respectively; and G and L are the single-pass gain and losses. Knowing that,

$$\Theta = \Theta_0 G^{\sigma_0^p/(\sigma_{em}-\sigma_1^L)} G^{-2r} \text{ with } \Theta_0 = e^{-\sigma_0^p N_0 d} \ , \tag{7}$$

$$P_{abs} \cong (1-\Theta_0) P_{inc} \ , \tag{8}$$

$$G = L^{-1} = \left[1 - \frac{T}{2} - \delta\right]^{-1} \ , \tag{9}$$

where δ gathers all the intracavity losses other than that of the output mirror transmission and r is a dimensionless parameter that measures the relative magnitude of the ESA and of the stimulated-emission cross sections and is given by

$$r = \frac{\sigma_1^p}{\sigma_{em} - \sigma_1^L} \ . \tag{10}$$

If the losses and the output mirror transmission are small compared to 1, which is generally the case with cw lasers, expressions (4) and (6) for the threshold pump power and the laser slope efficiency become

$$\rho_{diff} = \frac{h\nu_L}{h\nu_p} \frac{\sigma_{em} - \sigma_1^L}{\sigma_{em} + \sigma_1^L} \frac{T}{T+\delta}(1-F) \ , \tag{11}$$

$$P_{abs}^{th} = \frac{Sh\nu_p}{2(\sigma_{em} - \sigma_1^L)\tau}(T+2\delta)(1-F)^{-1} \tag{12}$$

with

$$F = \frac{\Theta}{1-\Theta_0} \frac{(\sigma_0^p + \sigma_1^p)(T+2\delta)}{2(\sigma_{em} - \sigma_1^L)} \ . \tag{13}$$

If we write $S = \pi(\omega_p^2 + \omega_L^2)/2$ and assume that F is small, we find expressions close to those commonly used in the literature. From these expressions it is clear that the

effect of ESA in the stimulated-emission domain can be very important since it can reduce the laser slope efficiency and enhance the absorbed pump power at threshold very significantly.

To understand the influence of the other parameters, particularly ESA in the pumping domain, we have analyzed the threshold absorbed pump power and the laser slope efficiency as a function of the output mirror transmission by varying the value of the optical losses L, the parameter r, and the transparency Θ_0. The value of the ratio $\sigma_0^p/(\sigma_{em}-\sigma_1^L)$ has been fixed to 0.15 because it is the value that generally applies in the case of the diode-pumped 1.06-μm Nd^{3+}-doped laser materials. Moreover, this ratio does not play a significant role since no difference could be observed between the curves for values larger than about 0.05. The output mirror transmission has been varied from 0 to 25% (it is generally less than 10%), the optical losses from 0 to 10% (they are generally of the order of 1%), and we worked with transparency values of 5 and 20%. Figures 1–3 show the dependences of the laser slope efficiency and the threshold pump power on these parameters. From the curves of Figs. 1 and 2, it can be concluded that ESA in the pumping domain has a significant effect only for r values larger than 0.5 and for output mirror transmissions larger than 5%. In the case of a stimulated-emission cross section of a few 10^{-19} cm^2, it means that ESA in the pumping region will have to be of the same order of magnitude to significantly perturb the laser performance of the system. This influence is more pronounced as the optical losses and the transparency of the material are larger, but they are values for which the systems are not generally operating. From the curves of Fig. 3, it is found that ESA in the pumping domain is of little importance compared to that of the transparency Θ_0. For an output mirror transmission $T=10\%$, for instance, the absorbed pump power at threshold does not vary by more than about 3% between $r=0$ and 2, that is, for a very unfavorable case corresponding to $L=4\%$ and $\Theta_0=20\%$. This is negligible compared to the experimental uncertainties which are usually of the order of 10%.

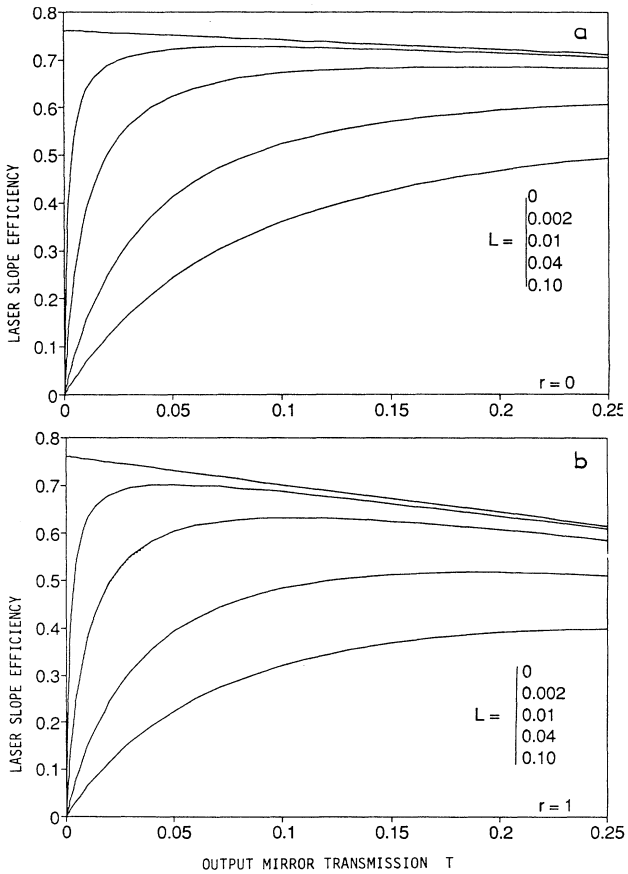

FIG. 1. Theoretical variations of the laser slope efficiency, ρ_{diff}, as a function of the output mirror transmission T for various values of the optical losses L and for (a) $r=0$ with $\Theta_0=5$ or 20% and (b) $r=1$ and $\Theta_0=5\%$.

B. Judd-Ofelt calibration of ESA spectra

The ESA cross sections between the energy levels of the rare-earth ions in the materials can be theoretically determined from an analysis of the classical GSA spectra by applying the well-known formalism developed by Judd and Ofelt.[13,14] In the case of ESA taking place in the Nd^{3+} metastable state $^4F_{3/2}$, the electric-dipole transition strengths will take the form

$$S(^4F_{3/2}\rightarrow J')=\sum_{t=2,4,6}\Omega_t|\langle {}^4F_{3/2}\|U^{(t)}\|J'\rangle|^2 , \tag{14}$$

where $U^{(t)}$ are matrix elements that can be found in the literature[18] and Ω_t are the so-called Judd-Ofelt parameters. Then the ESA spectra can be calibrated in units of cross sections by integrating them and writing

$$S_{calc}=\frac{\int\sigma_{ESA}(\lambda)}{\lambda}=C(n)S(^4F_{3/2}\rightarrow J') \tag{15}$$

with

$$C(n)=\frac{(n^2+2)^2}{9n}\frac{2\pi^3e^2}{3hc} \tag{16}$$

and $C(n)=0.0413$ for YAG ($n=1.82$), $C(n)=0.310$ for YLF ($n=1.455$), and $C(n)=0.0397$ for LMA ($n=1.77$).

The Ω_t parameters obtained with our own absorption data, as well as those found in the literature in the case of the Nd^{3+}-doped YAG, YLF, and LMA crystals studied in the following, are given in units of 10^{-20} cm^2 in Table I. The disagreements between the authors generally come from two sources or error: (1) from the method of calculation[25] which can give different results depending on whether transition strengths S or oscillator strengths f are used; (2) from the choice of the transitions entering in the calculation (for example, previous authors[21,23] found so low values for the parameter Ω_2 because they did not include the absorption transitions around 350 nm).

LMA(S) and LMA(NS) refer to two kinds of Nd^{3+}-doped $LaMgAl_{11}O_{19}$ (LMA) single crystals, near-stoichiometric (S) crystals of formula $LaMg_{0.7}Al_{11.2}O_{19}$ and nonstoichiometric (NS) congruent crystals of formula $La_{0.9}Mg_{0.5}Al_{11.433}O_{19}$ that were recently studied[16,17] for their particular optical and laser properties. In the following we shall use our own set of parameters (see Table I).

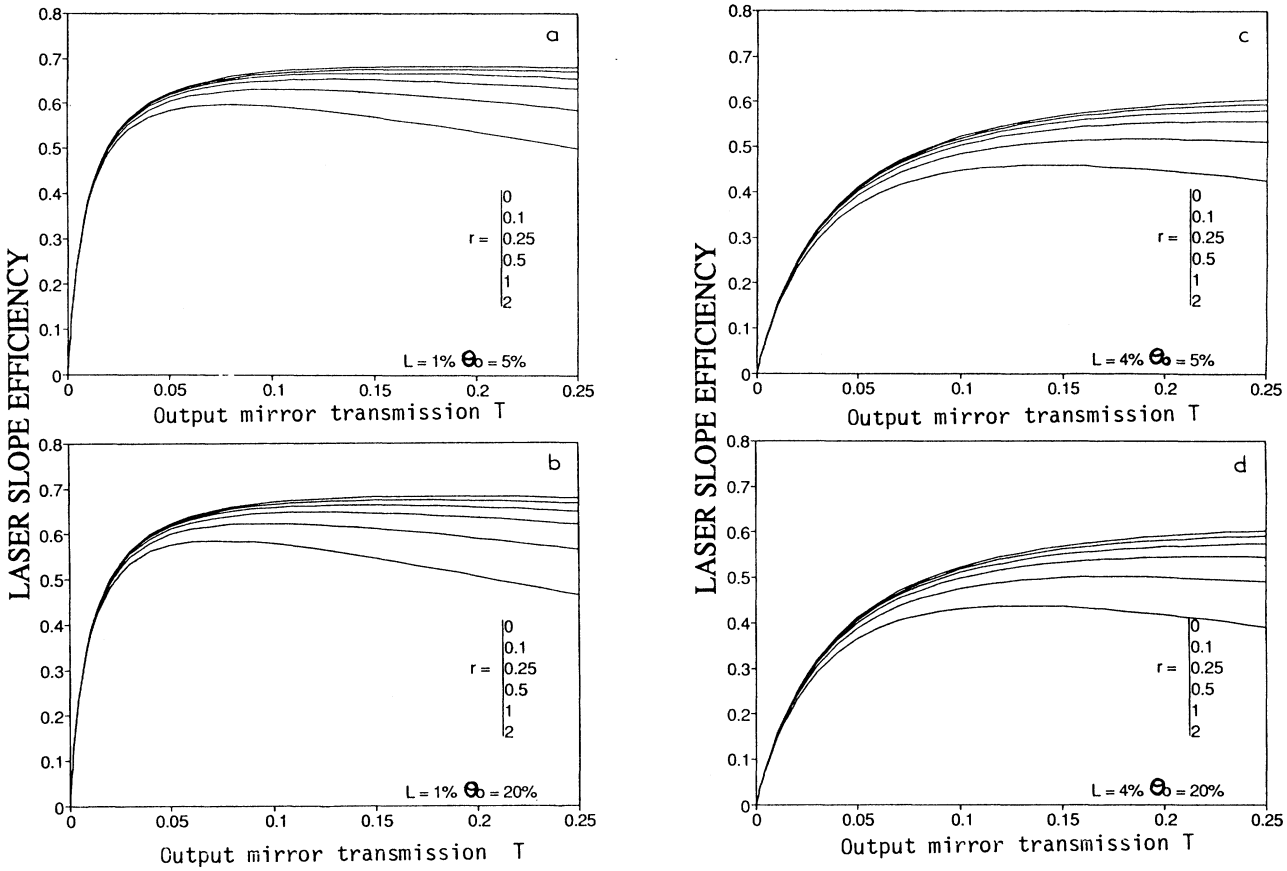

FIG. 2. Theoretical variations of the laser slope efficiency ρ_{diff} as a function of the output mirror transmission T for various values of r and for (a) $L=1\%$, $\Theta_0=5\%$; (b) $L=1\%$, $\Theta_0=20\%$; (c) $L=4\%$, $\Theta_0=5\%$; and (d) $L=4\%$, $\Theta_0=20\%$.

III. EXPERIMENTAL RESULTS AND ANALYSIS

A. Excited-state absorption

ESA processes can be often evidenced by the observation of some anti-Stokes visible fluorescences coming from levels lying at energies higher than the energy of the exciting photons. Recording of excited-state-excitation (ESE) spectra is then possible and it is what we have done more particularly to investigate ESA in the infrared-stimulated-emission domains. The experimental setup and results were given in Ref. 15. This method allows us to record highly resolved spectra (the resolution is that of the probe laser beam) and thus to accurately know the positions and the relative intensities of the ESA transition lines.

To calibrate these infrared spectra, we have used two methods. We have applied the Judd-Ofelt formalism by using the procedure previously described. We also have recorded portions of gain-ESA spectra directly. In this case, the pump laser beam was replaced by a flash lamp pump chamber and the samples to be studied were 7- or 9-cm-long laser rods of 6 or 7 mm in diameter, depending on the system. The probe beams were the ones which were already used in the previous ESE two-laser-beam experiments:[15] a pulsed YAG:Nd pumped dye laser associated with a hydrogen Raman cell (with Exciton dye Rh 590 around 1.06 μm and DCM around 1.32 μm). The intensity of the probe beam passing through the rod was detected by a Molectron pyroelectric detector and the signal fed into a Standard SR 250 analogical boxcar. The gain-ESA spectra are then given by

$$\ln(I_u/I_p)=(\sigma_{\text{ESA}}-\sigma_{\text{em}})N^*l\ , \tag{17}$$

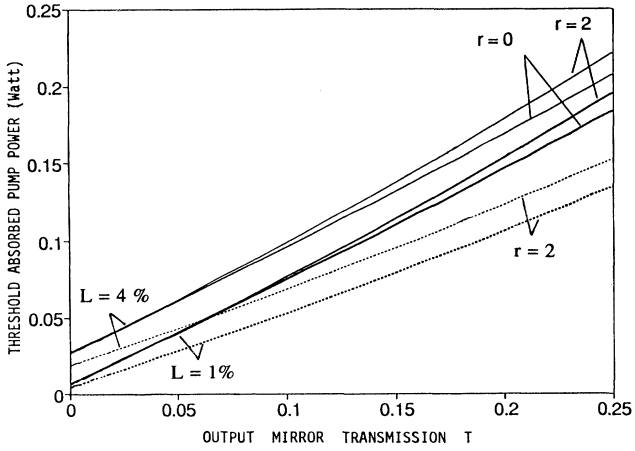

FIG. 3. Theoretical variations of the threshold absorbed pump power as a function of the output mirror transmission for $\Theta_0=5\%$ ($\cdots$) and $\Theta_0=20\%$ (——) and for different values of r and L.

TABLE I. Judd-Ofelt parameters (units of 10^{-20} cm^2) of Nd^{3+}-doped YAG, YLF, and LMA (near-stoichiometric *S* as well as nonstoichiometric *NS*).

	Ω_2	Ω_4	Ω_6	rms	Ref.
	0.37	2.29	5.97		19
YAG	0.2	2.7	5		20
	0	3.2	4.6		21
	0.32	3.0	5.16	0.16	This work
	1.9	2.7	5		22
YLF	0.36	4.02	4.84		23
	0.93	2.56	4.98	0.17	This work
LMA	1.23	1.75	2.24		24
(S)	1.12	1.79	1.80	0.10	This work
(NS)	1.34	1.84	2.03	0.11	This work

where I_p and I_u are the transmitted intensities of the probe beam through the rod of length l with and without pumping, respectively.

Then, knowing the stimulated emission cross section spectra $\sigma_{em}(\lambda)$ and the shape of the ESE spectra, the intensity of which $I_{ESE}(\lambda)$ is proportional to the ESA cross section, i.e., $I_{ESE}(\lambda)=\alpha\sigma_{ESA}(\lambda)$, we can find $\sigma_{ESA}(\lambda)$ by adjustment of the value of N^* and by writing

$$\sigma_{ESA}(\lambda)=\sigma_{em}(\lambda)-\ln(I_p/I_u)/N^*l=I_{ESE}(\lambda)/\alpha \ . \quad (18)$$

Concerning the ESA investigation in the visible and near-infrared pumping domains, we have recorded calibrated spectra more directly. The same kind of flash-lamp pump chamber was used as a pumping source in the case of Nd^{3+}-doped YAG and LMA but, because the YLF:Nd^{3+} laser rod was broken in the meantime and only reduced samples were available, we had to use another pulsed dye laser as pumping source for this system. The probe beam was that of a pulsed YAG:Nd pumped superradiant dye laser.[26] Indeed the special geometrical shape of the dye cuvette used in this experiment allowed us to obtain a broadband amplified fluorescence the divergence of which was weak enough to be collected into an optical fiber and to be sent efficiently through the YAG or the LMA laser rod or the YLF sample. At the output of the crystal, the transmitted light was collected by another fiber, sent onto the entrance slit of a Jobin-Yvon HRS1 monochromator and analyzed with the help of a 512 pixels optical multichannel analyzer from EG & G covering about 15 nm. This detection system allowed us to register spectra with a good spectral resolution and also time-resolved spectra thanks to a synchronization system controlling the time of triggering of the flash pump and/or of the lasers. Then in the investigated pumping domains, we have recorded transient absorption spectra:

$$\ln(I_p/I_u)=(\sigma_{GSA}-\sigma_{ESA})N^*l \ . \quad (19)$$

This kind of spectra allows one to directly know the excited-state-absorption cross section as soon as the ground-state-absorption cross section, σ_{GSA}, is known at a wavelength for which ESA is negligible.

Thus, the next three subsections will present ESA results in the three following interesting domains:

(1) The infrared stimulated emission domains around 1.06 and 1.32 μm for which we shall just complete the already available data by experimental and/or theoretical calibrations of the ESA spectra in a cross-section unit.

(2) The visible domain around 470 and 610 nm because these wavelengths correspond to strong ESA transitions, $^4F_{3/2}\rightarrow{}^2H_{9/2}$ and $^4F_{3/2}\rightarrow{}^4D_{3/2}$, respectively, and also because the GSA in these regions is relatively weak. These ESA transitions were already reported by Caird *et al.*[27] in a study about transient absorption due to color centers in YAG:Nd^{3+} and Nd^{3+}-doped phosphate glasses. As we shall see, we are reporting here much better resolved spectra. Another reason to study the red $^4F_{3/2}\rightarrow{}^4D_{3/2}$ ESA transition is, as mentioned above, its interest in photon avalanche processes which were reported recently.[4-6]

(3) The laser diode pumping domain around 800 nm. As we shall see, because the GSA intensities were too strong, we were unable to measure ESA experimentally in this domain. Thus we have built ESA spectra theoretically, knowing the ESA line positions, which can be calculated from the positions of the Stark components of the energy levels involved in the transitions and which are given in the literature for each compound[28-30] and using the Judd-Ofelt formalism, as described previously.

1. ESA in the infrared emission domains around 1.06 and 1.32 μm

In Ref. 15, we reported polarized excited-state-excitation spectra around 1.06 and 1.32 μm which correspond to

$$^4F_{3/2}\rightarrow{}^2G_{9/2}+(^2D_{3/2}+{}^4G_{11/2}+{}^2K_{15/2})$$

and $^4F_{3/2}\rightarrow{}^4G_{7/2}$ ESA transitions, respectively. The manifolds that appear between parentheses cannot be distinguished from the $^2G_{9/2}$ level in Nd^{3+}-doped YAG and LMA, whereas in YLF:Nd^{3+} the $^4F_{3/2}\rightarrow{}^2G_{9/2}$ transition is well determined. Figure 4 recalls the energy levels of the Nd^{3+} ion and the transitions of interest here.

In each material, we had already noticed that the ESA intensities, for a given polarization, was very weak at the laser wavelengths, around 1.06 μm ($^4F_{3/2}\rightarrow{}^4I_{11/2}$) as well as around 1.32 μm ($^4F_{3/2}\rightarrow{}^4I_{13/2}$). Now we are go-

ing to give the maximum ESA peak cross sections and the ESA cross sections at the laser wavelengths.

The calibration of the ESA spectra around 1.32 μm was only made with the Judd-Ofelt (JO) formalism[13,14] because it was too difficult to extract information from the ESA-gain spectra that were disrupted by the rotation-vibration water absorption in this region. According to the literature[18] the strength of the $^4F_{3/2} \rightarrow {}^4G_{7/2}$ intermanifold transition should not depend on the Ω_6 parameter, the selection rule being $|J-J'| \leq t \leq J+J'$ with $J=\frac{3}{2}$, $J'=\frac{7}{2}$ and is given by

$$S(^4F_{3/2} \rightarrow {}^4G_{7/2}) = 0.1064\Omega_2 + 0.0629\Omega_4 , \quad (20)$$

where the JO parameters Ω_t are those reported in Sec. II.

If E is the area of the polarization-averaged ESE spectra $I^p_{\mathrm{ESE}}(\lambda)$ with $p=\pi$ and σ in the case of YLF and LMA, we have

$$E = \frac{\int [2I^{\sigma}_{\mathrm{ESE}}(\lambda) + I^{\pi}_{\mathrm{ESE}}(\lambda)] d\lambda}{3\bar{\lambda}} , \quad (21)$$

where $\bar{\lambda}$ is the average wavelength of the transition.

The ESA cross section is simply calculated for each polarization by using the expression

$$\sigma^p_{\mathrm{ESA}}(\lambda) = (S_{\mathrm{calc}}/E) I^p_{\mathrm{ESE}}(\lambda) , \quad (22)$$

where S_{calc} is given by $S_{\mathrm{calc}} = C(n)S$ and $C(n)$ is given by expression (16).

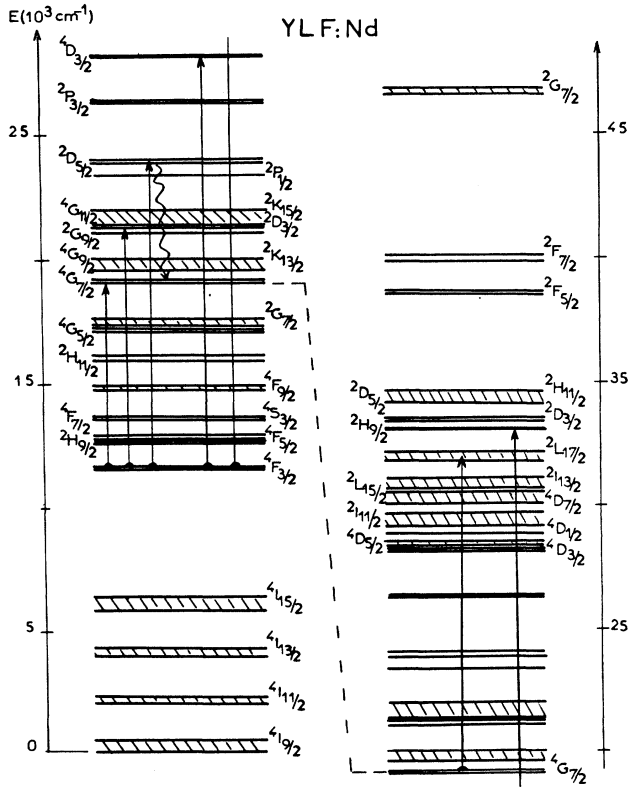

FIG. 4. Energy level diagram of Nd^{3+} (case of $YLiF_4$) and ESA transitions studied in this work.

The peak ESA cross sections so calculated are gathered in Table II. In the case of LMA, the large uncertainty on the calculated values comes from the poor knowledge of the terminal levels, $^4G_{7/2}$ or $^4G_{9/2}$, of the ESA transitions around 1.32 μm. With these values we thus find that the ESA cross sections at the laser wavelengths remain very weak: less than 10^{-21} cm^2 for YLF at 1.314 μm in σ and 1.321 μm in π polarization and for LMA at 1.300 and 1.378 μm in σ polarization, less than 0.5×10^{-21} cm^2 at 1.318 μm and about 2.5×10^{-21} cm^2 at 1.338 μm in YAG.

Around 1.06 μm the calibration with the Judd-Ofelt formalism is less accurate than around 1.32 μm because the terminal level of the ESA transition around 1.06 μm can participate of several multiplets and also because the recorded ESE spectra do not cover the entire

$$^4F_{3/2} \rightarrow {}^2G_{9/2} + {}^2D_{3/2} + {}^4G_{11/2} + {}^2K_{15/2}$$

ESA transitions. It is the case for YAG and LMA. Thus, the confrontation of the two methods of calibration described above was only really reliable in the case of YLF because the observed ESA lines are assigned to the only $^4F_{3/2} \rightarrow {}^2G_{9/2}$ ESA transition.

If we only take this $^4F_{3/2} \rightarrow {}^2G_{9/2}$ ESA transition into account for the three systems, we know that its strength does not depend on the Ω_2 parameter and is given by[18]

$$S(^4F_{3/2} \rightarrow {}^2G_{9/2}) = 0.0213\Omega_4 + 0.0316\Omega_6 . \quad (23)$$

Following the above procedure, the maxima of ESA cross sections in YLF were found to be 3.3×10^{-20} cm^2 at 1.051 μm in π polarization and 1.75×10^{-20} cm^2 at 1.048 μm in σ polarization. Using expression (18), the YLF-polarized gain-ESA spectra which are shown in Fig. 5, and the values of the stimulated-emission cross section peaks at 1.047 and 1.053 μm found in the π and σ polarizations and which were reported in the literature,[31] i.e., 3.7×10^{-19} and 2.6×10^{-19} cm^2, respectively, we have been led to maximum ESA cross sections of 7×10^{-20} and 4×10^{-20} cm^2 at 1.051 and 1.048 μm in the π and σ polarizations, respectively.

These values are about two times larger than those calculated with the first method. This factor cannot be explained with only the experimental errors; two explanations can be considered: The Judd-Ofelt formalism is not reliable when high-energy levels are involved. This explanation is not completely satisfactory because the $^2G_{9/2}$ level is only lying at about 21 000 cm^{-1} and because, as we shall see in the following, a good result has been obtained for an ESA transition terminating on an energy level lying at about 28 000 cm^{-1}. The calibration of the

TABLE II. Peak ESA cross sections (units of 10^{-20} cm^2) in Nd^{3+}-doped YAG, YLF, and LMA around 1.32 μm.

System	λ (μm)	σ^p_{ESA} (10^{-20} cm^2)
YAG	1.352	$\approx$1.0
YLF ($p=\pi$)	1.310	$\approx$1.9
YLF ($p=\sigma$)	1.328	$\approx$0.7
LMA ($p=\pi$)	1.310	0.9–2.0
LMA ($p=\sigma$)	1.310, 1.325	0.5–1.1

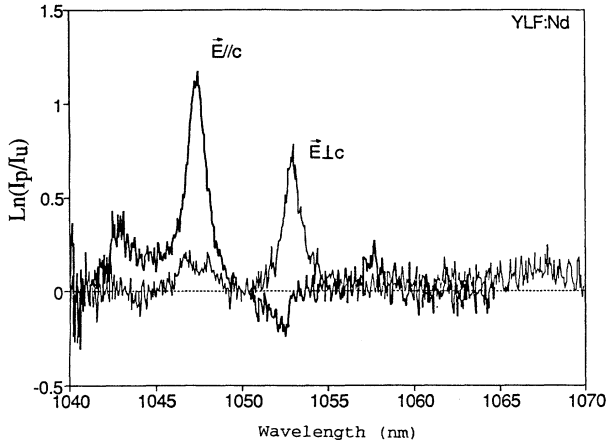

FIG. 5. Polarized gain-ESA spectra of YLF:Nd^{3+} recorded at $T=300$ K around 1.06 μm.

gain-ESA spectra is not good, leading us to reconsider the stimulated-emission cross sections found in the literature. This appears to make sense since these values, which result from laser experiments, are certainly too large by comparison with the values obtained from the calibration of the emission spectra $I^p_{em}(\lambda)$ using the well-known expression[32]

$$\sigma^p_{em}(\lambda)=\frac{3\lambda^4\beta}{8\pi n^2 c\tau_{rad}}\frac{I^p_{em}(\lambda)}{\int[2I^\sigma_{em}(\lambda)+I^\pi_{em}(\lambda)]d\lambda}, \quad (24)$$

where τ_{rad} is the radiative lifetime and β the branching ratio of the considered emission transition. Indeed, by using this expression, the maximum stimulated-emission cross sections at 1.047 and 1.053 μm are found to be equal to 1.8×10^{-19} and 1.4×10^{-19} cm^2 in the π and σ polarizations, respectively (if the Boltzmann factors[33] are taken into account, however, we again find values close to the previous ones, i.e., 4.1×10^{-19} and 2.4×10^{-19} cm^2). With these values the calibration of the gain-ESA spectra leads to ESA cross sections, σ^π_{ESA} (1.051 μm)$=3.7\times10^{-20}$ cm^2 and σ^σ_{ESA} (1.048 μm)$=1.9\times10^{-20}$ cm^2, in much better agreement with those obtained with the help of the Judd-Ofelt formalism. At any rate, independently of the chosen stimulated-emission cross sections of the laser transitions at 1.047 and 1.053 μm in Nd^{3+}-doped YLF, they are about 60 and 100 times stronger than the ESA cross sections at the same wavelengths in the same polarizations.

In the case of YAG:Nd^{3+}, depending on the terminal levels of the ESA transitions which are taken into account ($^2G_{9/2}$ alone or with $^4G_{11/2}$) in the Judd-Ofelt treatment, the estimated maximum ESA cross section at 1.074 μm is found between 3 and 11×10^{-20} cm^2. On the other hand, by using a stimulated-emission cross section of 7.4×10^{-19} cm^2 at 1.064 μm,[34] the gain-ESA calibration gives an ESA cross-section value at 1.074 μm of 10×10^{-20} cm^2, in good agreement with the Judd-Ofelt prediction. As a consequence ESA at the 1.064-μm laser wavelength is negligible.

In the case of LMA:Nd^{3+}, the maximum peak ESA cross section at 1.049 μm in the π polarization is estimated to be about 1.2×10^{-20} cm^2 by using the JO treatment and 1.5×10^{-20} cm^2 by using the gain-ESA spectra. The stimulated-emission cross section that was used here was an average of the values found in two kinds of LMA crystals[17] by other gain measurements, i.e., 5.9×10^{-20} cm^2 at about 1.0545 μm in the σ polarization. Here again ESA at the 1.0545-μm laser wavelength in the σ polarization can be neglected.

2. *ESA spectra around 610 and 470 nm*

(a) Case of YAG:Nd^{3+}. Figure 6 shows the room-temperature difference absorption spectra $\ln(I_u/I_p)$ which were recorded in YAG:Nd^{3+} from 590 to 625 nm and from 440 to 480 nm for the same excitation pump power. As in the case of the ESE spectra in the infrared domain, these spectra are made up of several lines the positions of which are in very good agreement with the ones calculated from the Nd^{3+} energy level diagram for this material. In the first range, we clearly distinguish the $^4F_{3/2}\rightarrow{}^4D_{5/2}$ from the $^4F_{3/2}\rightarrow{}^4D_{3/2}$ ESA transitions. The most intense line is lying at 619.4 nm and the shoulder on its short-wavelength side well corresponds to an

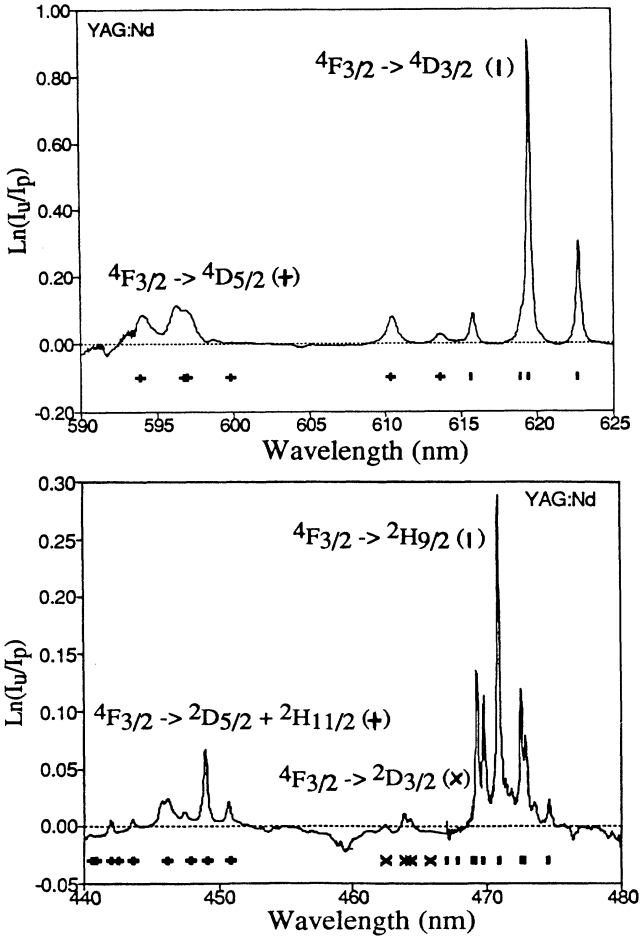

FIG. 6. Difference absorption spectra of YAG:Nd^{3+} recorded at $T=300$ K around 620 and 470 nm.

expected line. In the second range, we observe the following ESA transitions: $^4F_{3/2}\rightarrow{}^2D_{3/2}+{}^2H_{11/2}$ around 445 nm, $^4F_{3/2}\rightarrow{}^2D_{5/2}$ around 465 nm, and $^4F_{3/2}\rightarrow{}^2H_{9/2}$ around 470 nm. For this last transition, six lines over ten theoretically expected can be clearly observed. The ones expected at 467.0 and 467.8 nm are certainly too weak to be observed. On the other hand, the most intense line at 470.9 nm is in fact made of two overlapping ones and a line at 468.87 nm is probably also overlapping with that found at 469.08 nm. The wavelengths of both the $^4F_{3/2}\rightarrow{}^4D_{3/2}$ and $^4F_{3/2}\rightarrow{}^2H_{9/2}$ ESA transitions and their assignments are gathered in Table III.

The negative parts of the spectra correspond to GSA lines or backgrounds; they express bleaching processes due to depletions of the number of ions in the ground state. Most of these GSA lines are saturated (at 459 nm for instance), which means that the probe beam at these wavelengths is almost fully absorbed by the rod ($l\approx 8$ cm) and that the ratio I_u/I_p is not reliable. However at some other weak GSA wavelengths λ_a for which ESA is negligible, we can estimate the product N^*l by using the GSA cross section $\sigma_{\mathrm{GSA}}(\lambda_a)$ and the expression derived from expression (19):

$$N^*l=\frac{-\ln(I_u/I_p)(\lambda_a)}{\sigma_{\mathrm{GSA}}(\lambda_a)} . \tag{25}$$

Then we can use this factor to "directly" calibrate the difference absorption spectra $\ln(I_u/I_p)$ in cross-section units. In our experiment, the number of excited Nd^{3+} ions was about 10^{18} ions/cm^3, which corresponded to about 0.75% of the total density of Nd^{3+} ions in our 1 at. % Nd^{3+}-doped YAG crystal. The peak ESA cross section is found

$$\sigma_{\mathrm{ESA}}(470.9\ \mathrm{nm})=(3.6\pm1.2)\times10^{-20}\ \mathrm{cm}^2 ,$$

$$\sigma_{\mathrm{ESA}}(619\ \mathrm{nm})=(10.8\pm3.3)\times10^{-20}\ \mathrm{cm}^2 .$$

As in the previous section the difference absorption spectra also can be calibrated with the help of the JO formalism, but it is a little less direct than in the case of the ESE spectra because GSA has to be taken into account. The ESA cross-section spectra can now be obtained by using the expression

TABLE III. Wavelengths of the main $^4F_{3/2}\rightarrow{}^4D_{3/2}$ and $^4F_{3/2}\rightarrow{}^2H_{9/2}$ ESA transitions found or expected around 620 and 470 nm in YAG:Nd^{3+} and positions of the involved energy levels.

$^2H_{9/2}$ \ $^4F_{3/2}$	11 427 cm^{-1}	11 512 cm^{-1}
32 613 cm^{-1}	472.01 nm	473.91 nm
32 662 cm^{-1}	470.92 nm	472.81 nm
32 745 cm^{-1}	469.08 nm	470.96 nm
32 802 cm^{-1}	467.83 nm	469.70 nm
32 840 cm^{-1}	467.01 nm	468.86 nm
$^4D_{3/2}$ \ $^4F_{3/2}$		
27 571 cm^{-1}	619.43 nm	622.70 nm
27 670 cm^{-1}	615.65 nm	618.89 nm

$$\sigma_{\mathrm{ESA}}^{\mathrm{calc}}(\lambda)=(S_{\mathrm{calc}}-A)\Delta g(\lambda)/G+\sigma_{\mathrm{GSA}}(\lambda) , \tag{26}$$

where $\Delta g=\ln(I_u/I_p)$, $G=\int\Delta g(\lambda)d\lambda/\bar{\lambda}$, and $A=\int\sigma_{\mathrm{GSA}}(\lambda)d\lambda/\bar{\lambda}$, the limits of integration for G and A being the same and being chosen so as to cover the considered ESA transition, and where S_{calc} is calculated by using expression (15) and the JO parameters given in Sec. II.

In the case of the YLF and LMA uniaxial crystals, we also have to take into account for expression (26) the weights of $\frac{2}{3}$ and $\frac{1}{3}$ of the polarizations σ and π in the integrals G and A. If the oscillator strength of the $^4F_{3/2}\rightarrow{}^2H_{9/2}$ ESA transitions does not depend of the Ω_2 parameter, the oscillator strength of the $^4F_{3/2}\rightarrow{}^4D_{3/2}$ ESA transition only depends on this parameter and S_{calc} are given by

$$S(^4F_{3/2}\rightarrow{}^2H_{9/2})=0.0168\Omega_4+0.0064\Omega_6 \tag{27}$$

and

$$S(^4F_{3/2}\rightarrow{}^4D_{3/2})=0.1462\Omega_2 . \tag{28}$$

The peak ESA cross sections in YAG:Nd^{3+} are now found to be equal to 1.1×10^{-20} and 1.7×10^{-20} cm^2 at 470.9 and 619.4 nm, respectively. Thus, these "theoretical" values are about three and six times weaker than the experimental ones. If the first disagreement can be explained in part by the experimental errors, especially in the determination of N^*l from the very weak intensity of the GSA lines, the reason for the second one must probably be found in the error made in the derivation of the Ω_2 parameter, especially in YAG:Nd^{3+} in which it is about 50% according to Krupke,[20] but it is probably more important.

(b) Case of LMA:Nd^{3+}. Concerning LMA:Nd^{3+}, we have proceeded in the same way, but contrary to the case of YAG and YLF (presented below), the theoretical positions of the high-lying energy levels thus of the corresponding ESA lines are not well known. Furthermore, as is shown in Fig. 7, the lines in this material are much broader. Nevertheless, in each region, we can distinguish ten lines (numbered 1 to 10) which correspond to the number of expected lines for each $^4F_{3/2}\rightarrow{}^4D_{3/2}+{}^4D_{5/2}$ and $^4F_{3/2}\rightarrow{}^2H_{9/2}$ intermanifold ESA transition around 605 and 465 nm, respectively. These spectra allow us to determine a repetitive energy level spacing of about 120 cm^{-1} which we assign to the energy splitting of the two Stark components of the $^4F_{3/2}$ multiplet. This value is smaller than that usually reported in the literature[8] but this disagreement can be explained by the width of the ESA lines ($\Delta\nu\approx50$ cm^{-1}) and also by the multisite nature of this LMA system.[17]

Assuming a $^4F_{3/2}$ energy splitting of the order of 120 cm^{-1} the positions of the ESA lines can be used in turn to determine the energies of the terminal levels of the associated ESA transitions, of $^4D_{3/2}$ and $^4D_{5/2}$ for ESA around 605 nm and of $^2H_{9/2}$ (and probably $^2D_{3/2}$) for ESA around 465 nm. These energies are all gathered in Table IV.

The calibration of the LMA:Nd^{3+} spectra was made by using two methods: (1) From the determination of

N^*l, knowing that it was very delicate because it was difficult to find a wavelength at which there is no ESA and not too strong GSA. The chosen wavelength was 475 nm where the GSA cross section is 4.1×20^{-22} and 2.4×10^{-22} cm^2 in the σ and π polarizations, respectively. Then, the ESA cross sections are calculated by using the expressions (19) and (25) and it is found

$$\sigma^{\sigma}_{\mathrm{ESA}}(468.8\ \mathrm{nm})=2.8\times10^{-21}\ \mathrm{cm}^2\ ,$$

$$\sigma^{\sigma}_{\mathrm{ESA}}(603.3\ \mathrm{nm})=8.3\times10^{-21}\ \mathrm{cm}^2\ ,$$

$$\sigma^{\pi}_{\mathrm{ESA}}(463.6\ \mathrm{nm})=1.1\times10^{-21}\ \mathrm{cm}^2\ ,$$

$$\sigma^{\pi}_{\mathrm{ESA}}(599.8\ \mathrm{nm})=5.8\times10^{-21}\ \mathrm{cm}^2\ .$$

Here, the experimental error is estimated to be 50% especially on the factor N^*l and also because of the choice of the level of zero intensity of the difference absorption spectra. (2) From the Judd-Ofelt formalism, we have calibrated the polarized spectra by totally integrating each band, between 590 and 625 nm and between 450 and 475 nm. The oscillator strength of the ESA transition corresponding to the first range is:

$$S(^4F_{3/2}\rightarrow{}^4D_{3/2}+{}^4D_{5/2})=0.2221\Omega_2+0.2460\Omega_4 \qquad (29)$$

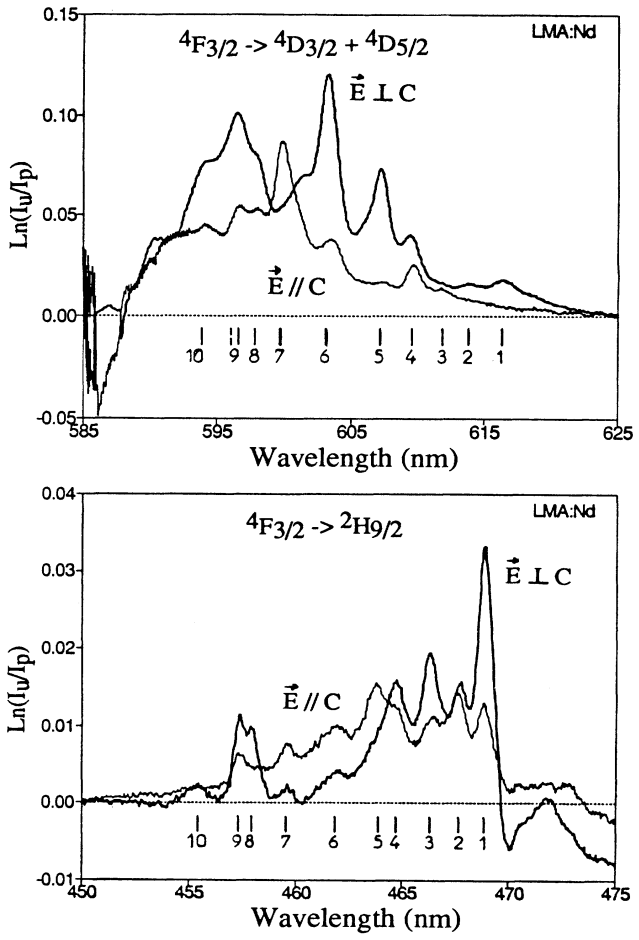

FIG. 7. Polarized difference absorption spectra of LMA:Nd^{3+} recorded at $T=300$ K around 605 and 465 nm.

TABLE IV. Wavelengths of the main $^4F_{3/2}\rightarrow{}^4D_{3/2}+{}^4D_{5/2}$ and $^4F_{3/2}\rightarrow{}^2H_{9/2}(^2D_{3/2})$ ESA transitions found experimentally around 605 and 465 in LMA:Nd^{3+} and tentative positioning of the corresponding energy levels.

$^4D_{3/2}+{}^4D_{5/2}$ \ $^4F_{3/2}$	11 580 cm^{-1}	11 700 cm^{-1}
27 923 cm^{-1}	616.4 nm (1)	611.9 nm (3)
27 989 cm^{-1}	609.5 nm (4)	613.9 nm (2)
28 160 cm^{-1}	603.3 nm (6)	607.4 nm (5)
28 370 cm^{-1}	596.5 nm (6)	599.8 nm (7)
28 427 cm^{-1}	593.7 nm (10)	597.9 nm (8)
$^2H_{9/2}+{}^2D_{3/2}$ \ $^4F_{3/2}$		
32 960 cm^{-1}	467.8 nm (2)	
33 030 cm^{-1}	468.8 nm (1), 466.3 nm (3)	
33 150 cm^{-1}	466.3 nm (3), 463.6 nm (5)	
33 220 cm^{-1}	464.8 nm (4), 462.0 nm (6)	
33 340 cm^{-1}	462.0 nm (6), 459.6 nm (7)	
33 450 cm^{-1}	459.6 nm (7), 457.4 nm (9)	
33 540 cm^{-1}	457.9 nm (8), 455.4 nm (10)	

and using expression (10), the results are

$$\sigma^{\sigma}_{\mathrm{ESA}}(603.3\ \mathrm{nm})=14.7\times10^{-21}\ \mathrm{cm}^2$$

and

$$\sigma^{\pi}_{\mathrm{ESA}}(599.8\ \mathrm{nm})=10.6\times10^{-21}\ \mathrm{cm}^2\ ,$$

thus in good agreement with the previous values, considering the approximations made and the experimental uncertainties.

Around 465 nm, the $^4F_{3/2}\rightarrow{}^2H_{9/2}$ ESA transition strength is given by expression (27) and that of $^4F_{3/2}\rightarrow{}^2D_{3/2}$ by

$$S(^4F_{3/2}\rightarrow{}^2D_{3/2})=0.0072\Omega_2\ . \qquad (30)$$

So, even if the latter is taken into account in the calibration—it represents about 15% of the former—we have found that the difference $(S_{\mathrm{calc}}-A)$ which is involved in expression (26) remains negative. So, in order to compare the results of the two methods we have proceeded in another way. We have first calibrated the spectra with the cross-section values found above and then we have compared the integrated cross sections. The integration of the difference absorption spectra from the value of N^*l leads to a value of 1.8×10^{-23} cm^2 and that of the GSA spectra in the same domain to 2.5×10^{-23} cm^2 which results in an ESA integrated cross section of 4.3×10^{-23} cm^2, a value about 2.5 times that of 1.7×10^{-23} cm^2 derived by the JO formalism. It is not so good as around 605 nm but it remains acceptable, taking into account the experimental uncertainties.

(c) Case of YLF:Nd^{3+}. As mentioned previously the YLF:Nd^{3+} crystal was excited by a pulsed YAG:Nd pumped dye laser instead of a flash lamp. The sample was a parallelepipedic crystal ($1.5\times4\times6$ mm^3) of YLF: 1.5% Nd^{3+} and it was excited at 585.3 nm (Exciton dye Rh 610). The resulting difference absorption spectra recorded in the π and σ polarizations around 595 and 465 nm are reported in Fig. 8.

Though these spectra are much more noisy than in the case of YAG:Nd^{3+}, especially around 465 nm, all the observed lines could have been identified. Only three lines at 464.5, 465.7, and 466.9 nm among ten could have been observed and assigned to $^4F_{3/2} \rightarrow {}^2H_{9/2}$ ESA transitions, probably because GSA is more intense than ESA at the other wavelengths. Similarly, among the four lines which are expected for the $^4F_{3/2} \rightarrow {}^4D_{3/2}$ ESA transition around 602 nm, only two of them at 601.62 and 603.64 nm have been distinguished. The expected line at 599.31 nm is probably hidden in the band corresponding to the broader $^4F_{3/2} \rightarrow {}^4D_{5/2}$ ESA transition located around 595 nm, and the intensity of the line expected at 605.59 nm is probably too weak to be detected. The positions of these lines and the energies of the levels involved in the ESA transitions are gathered in Table V.

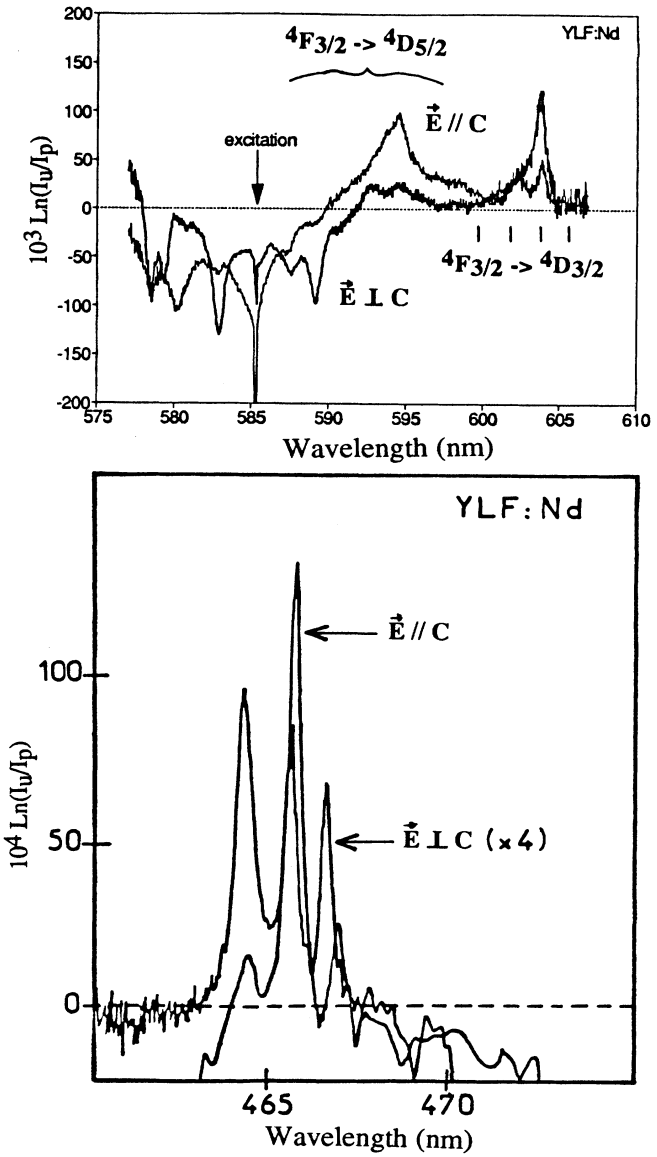

FIG. 8. Polarized different absorption spectra of YLF:Nd^{3+} at $T=300$ K around 595 and 465 nm.

TABLE V. Wavelengths of the main $^4F_{3/2} \rightarrow {}^4D_{3/2}$ and $^4F_{3/2} \rightarrow {}^2H_{9/2}$ ESA transitions found experimentally around 605 and 465 nm in YLF:Nd^{3+} and positions of the involved energy levels.

$^4D_{3/2}$ \ $^4F_{3/2}$	11 543 cm^{-1}	11 598 cm^{-1}
28 109 cm^{-1}	603.64 nm	(605.59 nm)
28 220 cm^{-1}	(599.31 nm)	601.62 nm
$^2H_{9/2}$ \ $^4F_{3/2}$		
33 016 cm^{-1}	465.7 nm	466.9 nm
33 072 cm^{-1}	464.5 nm	465.7 nm

Because the sample does not absorb too much, the GSA lines corresponding to the $^4I_{9/2} \rightarrow {}^2G_{7/2} + {}^4G_{5/2}$ transition appear distinctly and are not saturated. So it is easier to estimate the factor N^*l. Moreover the resulting calculated density of excited ions, $N^* \approx 1.3 \times 10^{18}$ ion/cm^3, is in good agreement with the value which is calculated by knowing the absorbed energy in the crystal, i.e., $N^* \approx 1.05 \times 10^{18}$ ions/cm^3. Knowing the GSA cross sections $\sigma_a^{\sigma} \approx \sigma_a^{\pi} \approx 2 \times 10^{-22}$ cm^2, the π and σ polarized ESA cross sections at 603.6 nm are

$$\sigma_{\mathrm{ESA}}^{\sigma}(603.3 \text{ nm}) = 0.65 \times 10^{-20} \text{ cm}^2$$

and

$$\sigma_{\mathrm{ESA}}^{\pi}(603.6 \text{ nm}) = 1.6 \times 10^{-20} \text{ cm}^2 .$$

For this ESA transition, the calibration with the Judd-Ofelt formalism gave ESA cross sections in very good agreement with these values, i.e., 0.84 and 1.9×10^{-20} cm^2 in the π and σ polarizations, respectively.

As we mentioned previously, it is precisely the $^4F_{3/2} \rightarrow {}^4D_{3/2}$ ESA transition which is involved in the photoavalanche process recently evidenced in YLF:Nd^{3+}. This process is operating at low temperature and necessitates the presence of a very efficient ESA at a wavelength where GSA is very weak. According to Fig. 8 and the previous calculations, we note that at room temperature this ESA should be more efficient in π polarization than in σ, whereas the avalanche mechanism was operating at low temperature in σ polarization. It seems that between low and room temperature, there is an inversion between the ESA intensities at 603.64 nm. The same temperature effect is known to occur on the $^4F_{3/2} \rightarrow {}^4I_{11/2}$ emission transition and very recently[35] we recorded ESA spectra around 600 nm which confirmed this effect. Moreover, Joubert *et al.*[6] worked out a simple rate equations model which was previously proposed in the case of Ni^{2+}-doped $CsCdCl_3$ (Ref. 36) and they estimated that the ESA cross section at 603.64 nm in σ polarization at 9 K is 3.2×10^{-20} cm^2, that is about five times larger than our experimental value at room temperature. Our recent results seem to confirm this but further experiments are necessary and are underway to evaluate this cross section accurately. A subsequent article will be devoted to these measurements and their analysis.

3. *ESA spectra around 800 nm*

When the crystals are pumped around 800 nm, a greenish white trace appears in the crystal, especially in the case of YLF:Nd^{3+}. These are anti-Stokes fluorescences issued from the $^4G_{7/2}$ level located around 19 000 cm^{-1} and also from the $^2P_{3/2}$ and $^4D_{3/2}$ emitting levels which are located around 27 000 cm^{-1}. They result from ESA and/or, as we shall see in the following section, from another kind of upconversion process which brings the excitation into these high-lying energy levels. An analysis of ESA was thus necessary. Unfortunately, as we already mentioned at the beginning, GSA in this wavelength domain is very strong and no significant ESA spectra could have been extracted. Consequently, we built calibrated ESA spectra by using the Judd-Ofelt formalism hoping that we could reach, as in the wavelength regions investigated previously, ESA cross sections with a good enough precision to decide the importance of this mechanism on the laser performance.

From the analysis of the energy level diagram of Nd^{3+}, after pumping around 800 nm the first ESA transition should occur between the levels $^4F_{3/2}$ and $^2D_{5/2}(1)$ (24 000 cm^{-1}) then, because of fast multiphonon relaxations, between the $^4G_{7/2}$ emitting level and the level $^2L_{17/2}$ (32 000 cm^{-1}). Thus we have built the ESA spectra corresponding to these two transitions and we have used for that the expression

$$\sigma_{\mathrm{ESA}}^{J-J'}(\lambda)=\bar{\lambda}S_{\mathrm{calc}}(J\rightarrow J') \times\sum_{i,j}\frac{f_i}{2J'+1}\frac{1}{\pi}\frac{\Delta\lambda/2}{(\lambda-\lambda_{ij})^2+(\Delta\lambda/2)^2}, \quad (31)$$

an expression in which we have assumed that all the transitions between the Stark components have the same intensity and the same polarization and where f_i is the Boltzmann factor of the Stark level No. i of the starting multiplet J of the ESA transition and that we have approximated by $1/(2J+1)$; $\Delta\lambda$ is the linewidth of the ESA lines, assumed with a Lorentzian profile and the same linewidth as the GSA lines around 800 nm, i.e., 1.5, 2, and 3 nm in YAG, YLF, and LMA, respectively; λ_{ij} are the expected wavelength positions of the ESA lines (because of the poor knowledge of the $^2L_{17/2}$ Stark levels in LMA, we have not reported the corresponding ESA transition); $\bar{\lambda}$ is the average wavelength of the transition $\bar{\lambda}\approx 8\times 10^{-5}$ cm; and $S_{\mathrm{calc}}(J\rightarrow J')$ is calculated by using again expression (15). Thus

$$S[^4F_{3/2}\rightarrow{}^2D_{5/2}(1)]=0.0010\Omega_2+0.0007\Omega_4 \quad (32)$$

and

$$S(^4G_{7/2}\rightarrow{}^2L_{17/2})=0.0192\Omega_6 . \quad (33)$$

The resulting ESA cross-section spectra are reported in Figs. 9–11 with the GSA spectra in the same wavelength domain.

The GSA transition lines more strongly overlap with the $^4F_{3/2}\rightarrow{}^2D_{5/2}(1)$ than with the $^4G_{7/2}\rightarrow{}^2L_{17/2}$ ESA transition and the cross sections of these various transitions differ by orders of magnitude with much smaller

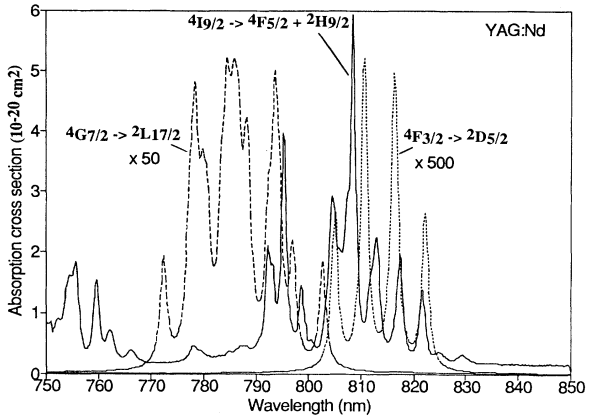

FIG. 9. GSA and calculated ESA cross-section spectra around 800 nm in YAG:Nd^{3+}.

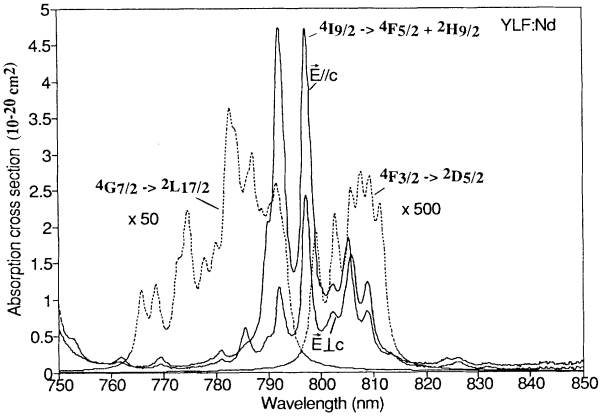

FIG. 10. Polarized GSA and calculated (nonpolarized) ESA cross-section spectra around 800 nm in YLF:Nd^{3+}.

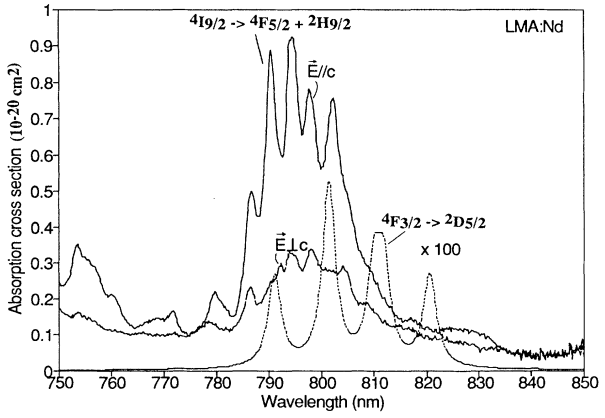

FIG. 11. Polarized GSA and calculated (nonpolarized) ESA cross-section spectra around 800 nm in LMA:Nd^{3+}.

values for the ESA than for the GSA transitions. We shall see in the following section that the relative positions and intensities of these spectra cannot give account alone of the anti-Stokes fluorescence excitation spectra which have been recorded in this domain.

B. Up-conversion effects

1. Anti-Stokes fluorescence excitation spectra around 800 nm

In this subsection we report and analyze excitation spectra which have been recorded by monitoring the anti-Stokes fluorescences mentioned above and by scanning the excitation with a homemade cw Ti:sapphire laser in the 800-nm region. A number of similar studies have been already devoted in the past to YAG:Nd^{3+},[11,37–39] YLF:Nd^{3+},[40] and other Nd^{3+}-doped materials,[41–43] but it is only recently, to our knowledge, that some results have been reported[44] for an excitation around 800 nm.

The monitored anti-Stokes fluorescences were orange and blue fluorescences around 590 and 400 nm which correspond to $^4G_{7/2} \rightarrow {}^4I_{11/2}$ and $(^4D_{3/2}, {}^2P_{3/2}) \rightarrow ({}^4I_{13/2}, {}^4I_{11/2})$ emission transitions, respectively. No blue fluorescence, however, was observed in YAG:Nd^{3+}. These fluorescences were analyzed with a Jobin Yvon HR250 monochromator and detected with a Hamamatsu photomultiplier. Depending on the dynamics of the studied fluorescence, an Ortec photon counting system or a Stanford boxcar integrator coupled with a computer completed the detection system.

We noted first that the dependence of the intensity of the orange and blue fluorescences on the excitation pump power was quadratic and cubic, respectively, as it is expected for two- and three-photon excitation processes. We report in Figs. 12–14 polarized excitation spectra which were obtained by monitoring the fluorescences coming from the infrared emitting level $^4F_{3/2}$ as well as from the high-lying levels $^4G_{7/2}$ (orange) and $^2P_{3/2}$ (blue) in order to follow the shape of these spectra with the order of the involved processes. From this point of view, about the same behavior was observed in the three systems, so only the case of YLF:Nd^{3+} will be analyzed hereafter.

The excitation spectra of the three fluorescences originating of the three $^4F_{3/2}$, $^4G_{7/2}$, and $^2P_{3/2}$ energy levels present peaks at the same positions. It means that the anti-Stokes fluorescences are not very sensitive to the excitation wavelength, as is expected for an ESA process provided that it is assisted by phonons. On the other hand, the lines become narrower, with widths of about 2.6, 2, and 1.6 nm, as the order of the excitation process increases. Finally these excitation spectra extend from 780 up to 810 nm while, according to the previous analysis, ESA should be significant only above 790 nm. This has led us to consider the occurence of upconversion excitation by energy transfers[45] which is more than possible, given the doping levels of the samples. We are thus tempted to analyze the results by using a four-level scheme in which we have assumed rapid multiphonon relaxations from levels 2 and 3 and upconversion en-

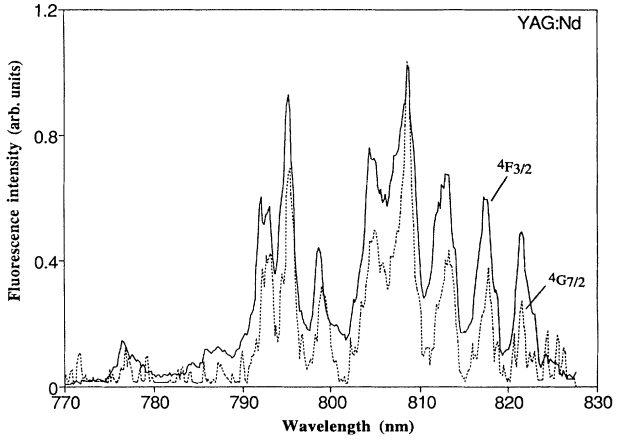

FIG. 12. Excitation spectra of the Stokes and anti-Stokes fluorescences coming from the levels $^4F_{3/2}$ and $^4G_{7/2}$ in YAG:Nd^{3+}.

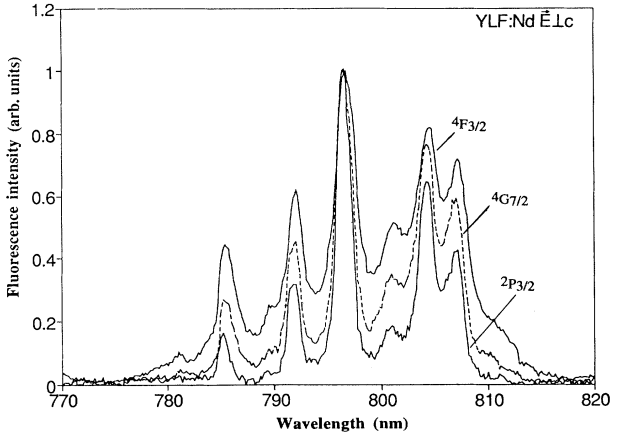

FIG. 13. σ-polarized excitation spectra of the Stokes and anti-Stokes fluorescences coming from the levels $^4F_{3/2}$, $^4G_{7/2}$, and $^2P_{3/2}$ in YLF:Nd^{3+}.

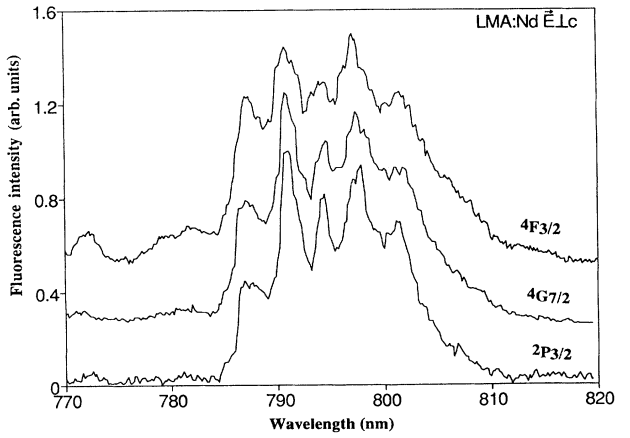

FIG. 14. σ-polarized excitation spectra of the Stokes and anti-Stokes fluorescences coming from the levels $^4F_{3/2}$, $^4G_{7/2}$, and $^2P_{3/2}$ in LMA:Nd^{3+}.

ergy transfers between adjacent ions bringing one ion in state 2 or state 3 from another one in state 1, and where σ_0 is the GSA cross section, σ_1 and σ_2 are the (phonon-assisted) ESA cross sections from levels 1 and 2, respectively, τ_2 and τ_3 are the fluorescence lifetimes of levels 2 and 3, W_{11} and W_{12} are the energy-transfer rates $(1,1)\rightarrow(0,2)$ and $(1,2)\rightarrow(0,3)$, respectively. In YLF:Nd^{3+} the energy-transfer processes which can be involved are

W_{11}: $(^4F_{3/2},{}^4F_{3/2})\rightarrow(^4I_{11/2},{}^2G_{9/2})$

and

$(^4F_{3/2},{}^4F_{3/2})\rightarrow(^4I_{13/2},{}^4G_{7/2})$,

W_{12}: $(^4F_{3/2},{}^4G_{7/2})\rightarrow(^4I_{9/2},{}^4D_{7/2})$,

$(^4F_{3/2},{}^4G_{7/2})\rightarrow(^4I_{11/2},{}^4D_{3/2})$,

and

$(^4F_{3/2},{}^4G_{7/2})\rightarrow(^4I_{13/2},{}^2P_{3/2})$.

The population equations for levels 2 and 3 can thus be written

$$\frac{dN_3}{dt}=\sigma_2 F N_2+W_{12}N_1N_2-N_3/\tau_3 , \tag{34}$$

and

$$\frac{dN_2}{dt}=\sigma_1 N_1+W_{11}N_1^2-N_2/\tau_2-\sigma_2 F N_2-W_{12}N_1N_2 , \tag{35}$$

where F is the excitation pump power.

In the steady state, the populations become

$$N_3^\infty=\tau_3(\sigma_2 F N_2^\infty+W_{12}N_1^\infty N_2^\infty) \tag{36}$$

and

$$N_2^\infty=\frac{\sigma_1 F N_1^\infty+W_{11}N_1^{\infty 2}}{\sigma_2 F+W_{12}N_1^\infty+1/\tau_2} \tag{37}$$

or by combining the previous expressions,

$$N_3^\infty=\tau_3\frac{\sigma_1 F N_1^\infty+W_{11}N_1^{\infty 2}}{1+1/(\sigma_2 F+W_{12}N_1^\infty)\tau_2} \tag{38}$$

and, in the case of weak excitation pump power, i.e., $\sigma_2\tau_2 F\ll 1$ and $W_{12}\tau_2 N_1^\infty\ll 1$,

$$N_3^\infty\approx\tau_2\tau_3[\sigma_1\sigma_2 F^2 N_1^\infty+(W_{11}\sigma_2+W_{12}\sigma_1)F N_1^{\infty 2}+W_{11}W_{12}N_1^{\infty 3}] . \tag{39}$$

So, as expected, if N_1^∞ varies linearly with the excitation pump power (in the case of weak dopant concentration and not too strong excitation power), the dependence with the excitation power of the intensity of the anti-Stokes fluorescence coming from the third emitting level will be cubic.

Moreover, if only the upconversion processes are involved in the feeding of levels 2 and 3, the spectral profile of N_3^∞ should vary like the cube of the spectral profile of N_1^∞. On the other hand, if the ESA cross sections σ_1 and σ_2 are not negligible, this profile will be modulated by the spectral shape of σ_1 and σ_2. The best fits of the excitation spectra of the anti-Stokes fluorescences issued from the $^4G_{7/2}$ and $^2P_{3/2}$ levels, with a power function of the excitation spectrum of the fluorescence coming from the $^4F_{3/2}$ metastable level, is obtained for

$$N_2(\lambda)=N_1(\lambda)^{1.68}$$

and

$$N_3(\lambda)=N_1(\lambda)^{2.31} .$$

As these values only slightly differ from 2 and 3, the upconversion energy transfers probably play an important role; it seems however ESA is far from being negligible. Thus we have tried to determine more particularly the contribution of ESA to the feeding of level $^4G_{7/2}$ by looking for the best set of parameters α and β such as

$$N_2(\lambda)=\alpha N_1(\lambda)+\beta N_1^2(\lambda) \tag{40}$$

with

$$\alpha=\tau_2\sigma_1 I\frac{N_1\max}{N_2\max}$$

and

$$\beta=\tau_2 W_{11}\frac{N_1^2\max}{N_2\max} .$$

The best fit was obtained for $\alpha\approx 0.3$ and $\beta\approx 0.7$. This model assumes that α, i.e., ESA, is independent of λ, which means, as mentioned above, that ESA is phonon assisted.

2. *Infrared fluorescence decay behavior*

The upconversion energy-transfer processes can also affect the fluorescence lifetime of the infrared metastable level. On the other hand, laser experiments[46] have shown that the effective fluorescence lifetime τ_e of this level is shorter than the expected value and shortens as the excitation pump power is increased. So we have studied the variation of this infrared fluorescence decay with the excitation pump power and have tried to relate the results with the upconversion energy-transfer mechanism discussed previously. First, we find that the fluorescence decay mode is exponential at weak excitation pump power but becomes more and more nonexponential when this excitation power increases. This is shown in Fig. 15 in the case of YLF:Nd^{3+}. To analyze this behavior, we have used again the energy level scheme worked above, but by only considering the three lower levels and by assuming no ESA. With these conditions the rate equation for the infrared emitting level No. 1 is

$$\frac{dN_1}{dt}=-N_1/\tau+W_{11}N_1^2 . \tag{41}$$

The solution of this Bernouilli equation is

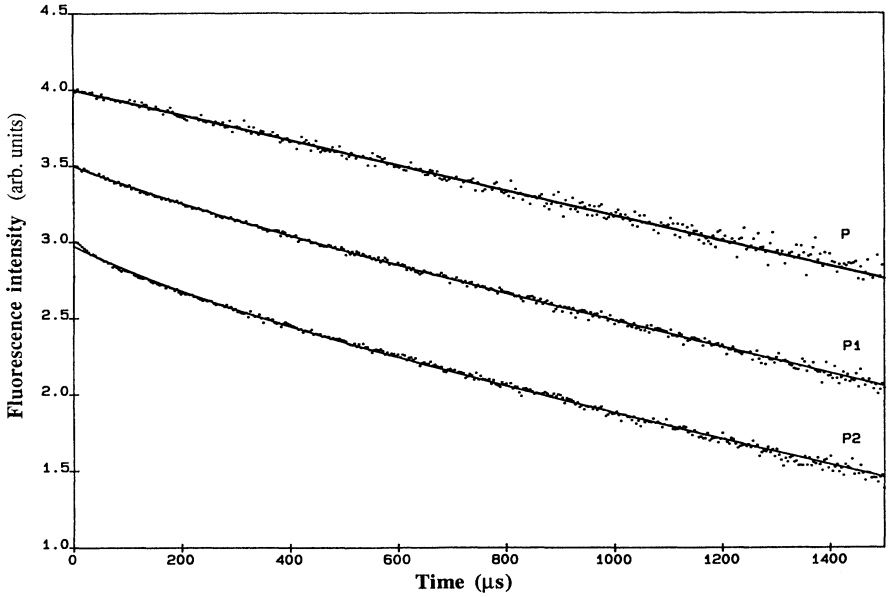

FIG. 15. Decay of the infrared fluorescence coming from level $^4F_{3/2}$ in YLF:Nd^{3+} for different excitation pump powers $P \ll P1 < P2$ and fits with expression (42) in the text.

$$N_1(t)=\left[-\tau W_{11}+\left[\frac{1}{N_1(0)}+\tau W_{11}\right]\exp(t/\tau)\right]^{-1}. \tag{42}$$

From this expression, we deduce the ratio between the effective lifetime τ_e for which $N_1(\tau_e)=N_1(0)/e$ and the fluorescence lifetime τ (at low pump power):

$$\frac{\tau_e}{\tau}=\ln\left[1+\frac{(e-1)}{1+N_1(0)W_{11}\tau}\right]. \tag{43}$$

Thus the decrease of the effective lifetime only depends on the product $N_1(0)W_{11}\tau$, i.e., of the pumping and upconversion rates and of the fluorescence lifetime. We report in Fig. 16 the variation of τ_e/τ as a function of $W_{11}N_1(0)$ in the case of YLF and YAG for which $\tau=550$ and 240 μs, respectively.

Knowing the excited ion density and the effective lifetime which is calculated from the decays, thus the ratio τ_e/τ, we have estimated from Fig. 16 the upconversion rates in YLF and YAG, $W_{11}=(1.7\pm1)\times10^{-16}$ and $(2.8\pm1)\times10^{-16}$ $cm^3\,s^{-1}$, respectively. In the end, we have fitted the decays according to expression (42) and adjusting W_{11}. The result is shown in Fig. 15 and the adjusted W_{11} values agree well with that found previously.

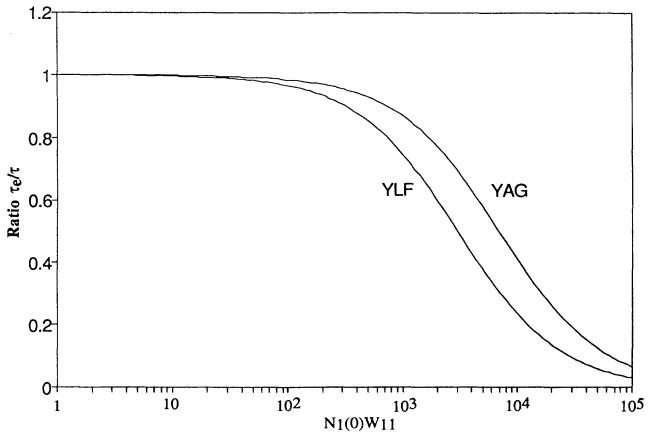

FIG. 16. Theoretical evolutions of the ratio τ_e/τ as a function of the parameter $W_{11}N_1(0)$ in the case of YAG:Nd^{3+} and YLF:Nd^{3+}.

IV. DISCUSSION/CONCLUSION

In the first part of this work we developed a very simple model to examine the influence of excited-state absorption, in the pumping as well as in the emission domains, on the laser performance of a four-level laser system in order to apply it in the case of Nd^{3+}-doped laser crystals. The effect of ESA in the emission domain is clearly detrimental for laser action. The effect of ESA in the pumping domain is less evident. In particular, the model shows that ESA will significantly perturb the laser performance of the Nd^{3+}-doped laser crystals if its cross section is of the same order of magnitude as that of the stimulated emission.

The second part of this work has been devoted to an experimental and theoretical analysis of ESA in Nd^{3+}-doped crystals of YAG, YLF, and LMA in the laser wavelength domains around 1.06 and 1.32 μm and in some specific excitation wavelength domains, around 460, 600, and 800 nm, because of their intervention in flashlamp and diode laser pumping and also in some particular photon-avalanche process. The experimental results have shown first that ESA in the infrared metastable level $^4F_{3/2}$ of Nd^{3+} in these crystals at the main laser wavelengths is negligible. So it cannot be invoked in these materials to account, for instance, for discrepancies that some authors could find between the net gain cross sections derived from laser experiments and the stimulated-emission cross sections determined from emission spectra. Then, the analysis of the ESA data in the laser as well as in the pumping domains within the framework of the Judd-Ofelt theory have shown that the ESA cross sections could be estimated, in most cases, to better than

50%, which is very satisfactory, considering the experimental uncertainties and the approximations made in this theory. Knowing that, we have found that ESA in the $^4F_{3/2}$ metastable state in the laser diode-pumping domain around 800 nm could occur but with much weaker cross sections than for GSA in the same domain, the latter being already much weaker than the stimulated-infrared-emission cross sections around 1.06 μm, with $\sigma_{GSA}(800\ nm) \approx 0.15\sigma_{em}(1.06\ \mu m)$ approximately. This is very important because, as stated above, ESA in the metastable state at the pumping wavelength can perturb the laser performance of the systems only if its cross section is of the same order of magnitude as that of the stimulated emission. Since it is not the case, we can conclude that ESA around 800 nm, at least in the metastable state, should not influence the laser performance significantly. Moreover, concerning ESA in the visible domain, which might be important for flash-lamp pumping, we have estimated theoretically that the integrated ESA cross section between 400 and 900 nm should not exceed 10% of the integrated GSA cross section in the same domain. So, the influence of ESA should be notable only for high excitation densities, as is the case in the high power flash-lamp-pumped system. In this case we could have shown indeed[47] the existence of increasing thermal effects—thermal lensing, thermal birefringence—when going from a stimulated-emission to a spontaneous-emission regime which can be explained for about one-third by the ESA mechanisms and the subsequent heating by the multiphonon relaxations.

ESA not being the essential mechanism for the reduced laser performances of the systems, we have invoked excitation and loss processes by upconversion energy transfers, first in the $^4F_{3/2}$ metastable state. This possibility has been analyzed and confirmed by recording in the 800-nm wavelength domain excitation spectra of anti-Stokes fluorescences coming from higher-lying emitting levels of Nd^{3+}, by discussing their profiles, and by comparing them to the ones expected theoretically. It has been invoked too to account for the reduction of the infrared metastable lifetime, as by Seelert *et al.*[46] to explain the reduced laser performance of their high-power YLF:Nd^{3+} laser. They determined a fluorescence lifetime of 410 μs, instead of 540 μs, for a cw excitation density of 800 W/cm^2 at around 800 nm. If we analyze the problem within the framework of the model that we have developed in the second part of our work, and which applies for pulsed excitation, the equivalent number of excited ions N_e^* is related to the pump power by the expression

$$N_e^* = P\alpha\tau/h\nu\ , \tag{44}$$

where α is the absorption coefficient at the pump wavelength and τ the fluorescence lifetime at low excitation pump powers. By using $\tau = 540\ \mu s$ and $P = 800$ W/cm^2 we find with our model $\tau_e/\tau \approx (0.7 \pm 0.15)$, thus $\tau_e \approx 385$ μs, in very good agreement with the above values.

Concerning the energy transfers which are involved for these upconversion phenomena we also have remarked from the ESA spectra recorded in the infrared domain that the only ESA transitions taking place in the metastable state which overlap with emission transitions are those terminating on the $^2G_{9/2}$ and $^4G_{7/2}$ levels around 1.06 and 1.32 μm, respectively; There is no overlap of any ESA transition from state $^4F_{3/2}$ with the emission transition $^4F_{3/2} \rightarrow {}^4I_{9/2}$ around 0.9 μm. Consequently the energy transfers are the following:

$$(^4F_{3/2}, {}^4F_{3/2}) \rightarrow (^4I_{11/2}, {}^2G_{9/2})$$

and

$$(^4F_{3/2}, {}^4F_{3/2}) \rightarrow (^4I_{13/2}, {}^4G_{7/2})\ .$$

To illustrate this point we have calculated the spectral overlaps of the respective ESA and emission cross sections in YAG and YLF:Nd^{3+} (averaging over polarization in the latter) and we have found $\int \sigma_{ESA}(\lambda)\sigma_{em}(\lambda)d\lambda = 3.2$ and 2.5×10^{-27} cm^4 s^{-1}, knowing that the contribution of the overlap around 1.06 μm is about 30 and 210 times larger than that around 1.32 μm, in YAG and YLF, respectively. The overlap in YAG is thus 1.2 times larger than that in YLF, which agrees well with the ratio of 1.6 found between the energy-transfer rates derived from the decay data.

In the end we can examine the solution which has been proposed recently[44] to identify the process responsible for the increasing inefficiency of a diode-pumped Q-switched Nd:YLF laser with decreasing pulse repetition rate. The proposition is an ESA transition at the laser emission wavelength taking place in the $^4G_{7/2}$ excited state after population of this state via the above upconversion energy transfers and subsequent multiphonon relaxations. We have calculated first the integrated cross section of the involved ESA transition and we have found $S_{calc}(^4G_{7/2} \rightarrow {}^4D_{5/2}) = 9.6 \times 10^{-23}$ cm^2, which is of the same order of magnitude as the $^4F_{3/2} \rightarrow {}^2G_{9/2}$ transition. So this could lead to ESA peaks with cross sections of the order of several 10^{-20} cm^2, which indeed could be detrimental for laser action at high pumping levels if one of these peaks coincided with a laser transition, and considering the energy scale of Nd in $YLiF_4$ (Ref. 29) this might be possible.

ACKNOWLEDGMENTS

Thanks are expressed to Dr. J. Y. Gesland (Université du Maine, Cristallogenèse, France), Dr. Ch. Wyon (LETI/CEA, Grenoble), and CRISMATEC S.A. for providing us with the YLF, LMA, and YAG crystals, respectively, and B. M. Industries for the flash-lamp pump chamber used in this study.

[1] M. Hemici, S. Mottin, M. Bon, J. Y. Roncin, and P. Laporte, J. Phys. III (France) **1**, 2061 (1991).

[2] R. Moncorgé and T. Benyattou, Phys. Rev. B **37**, 9177 (1988); **37**, 9186 (1988).

[3] H. Manaa, Y. Guyot, and R. Moncorgé, Phys. Rev. B **48**, 3633 (1993).

[4] J. S. Chivian, W. E. Case, and D. D. Eden, Appl. Phys. Lett. **35**, 124 (1979); A. W. Kueny, W. E. Case, and M. E. Koch, J.

Opt. Soc. Am. B **6**, 639 (1989); M. E. Koch, A. W. Kueny, and W. E. Case, Appl. Phys. Lett. **56**, 1083 (1990).
[5]W. Lenth and R. M. Macfarlane, J. Lumin. **45**, 346 (1990).
[6]M. F. Joubert, S. Guy, and B. Jacquier, Phys. Rev. B **48**, 10 031 (1993).
[7]Y. Guyot, R. Moncorgé, X. Banti, P. Laporte, and E. Mottay (unpublished).
[8]R. R. Petrin, M. L. Kliewer, J. T. Beasley, R. C. Powell, I. D. Aggarwal, and R. C. Ginther, IEEE J. Quantum Electron. **27**, 1031 (1991).
[9]S. Zemon, B. Petersen, G. Lambert, W. J. Miniscalco, B. T. Hall, R. C. Folweiler, W. A. Thompson, and L. J. Andrews, IEEE Phot. Tech. Lett. **4**, 244 (1992).
[10]P. R. Morkel, M. C. Farries, and S. B. Poole, Opt. Commun. **67**, 349 (1988).
[11]M. L. Kliewer and R. C. Powell, IEEE J. Quantum Electron. **25**, 1850 (1989).
[12]S. A. Payne, J. A. Caird, L. L. Chase, L. K. Smith, N. D. Nielsen, and W. F. Krupke, J. Opt. Soc. Am. B **8**, 726 (1991).
[13]B. R. Judd, Phys. Rev. **127**, 750 (1962).
[14]G. S. Ofelt, J. Chem. Phys. **37**, 511 (1962).
[15]Y. Guyot and R. Moncorgé, J. Appl. Phys. **73**, 8526 (1993).
[16]N. Mermilliod, R. Romero, I. Chartier, C. Garapon, and R. Moncorgé, IEEE J. Quantum Electron. **28**, 1179 (1992).
[17]Y. Guyot, C. Garapon, and R. Moncorgé, Opt. Mater. (to be published).
[18]W. T. Carnall, H. Crosswhite, and H. M. Crosswhite (unpublished).
[19]A. A. Kaminskii and L. Li, Phys. Status Solidi A **26**, K21 (1974).
[20]W. F. Krupke, IEEE J. Quantum Electron. **7**, 153 (1971).
[21]D. Knowles, A. Cassanho, and H. P. Jenssen, in *Tunable Solid State Lasers,* Vol. 5 of the OSA Proc. Series, edited by M. L. Shand and H. P. Jenssen (Optical Society of America, Washington, D.C., 1989), p. 139.
[22]W. F. Krupke, in *Proceedings of the IEEE Region IV Conference* (Institute of Electrical and Electronics Engineers, New York, 1974), p. 17.
[23]J. R. Ryan and R. Beach, J. Opt. Soc. Am. B **9**, 1883 (1992).
[24]B. Viana, D. Saber, A. M. Lejus, D. Vivien, R. Romero, and C. Wyon, in *Advanced Solid State Lasers,* Vol. 15 of the OSA Proc. Series, edited by A. Pinto and T. Y. Fan (Optical Society of America, Washington, D.C., 1993), p. 242.
[25]C. Li, Doctoral thesis, University of Lyon 1, 1992.
[26]J. Y. Roncin and H. Damany, Rev. Sci. Instrum. **52**, 1922 (1981).
[27]J. Caird, P. R. Staver, and K. S. Jancaitis (unpublished).
[28]J. B. Gruber, M. E. Hills, T. H. Allik, C. K. Jayasankar, J. R. Quagliano, and F. S. Richardson, Phys. Rev. B **41**, 7999 (1990).
[29]A. A. S. da Gama, G. F. de Sa, P. Porcher, and P. Caro, J. Chem. Phys. **75**, 2583 (1981).
[30]D. Saber, J. Dexpert-Ghys, P. Caro, A. M. Lejus, and D. Vivien, J. Chem. Phys. **82**, 5648 (1985).
[31]N. P. Barnes, D. J. Gettemy, L. Esterowitz, and R. E. Allen, IEEE J. Quantum Electron. **QE23**, 1434 (1987).
[32]T. M. Pollack, W. F. Wing, R. J. Grasso, E. P. Chicklis, and H. P. Jenssen, IEEE J. Quantum Electron. **QE18**, 159 (1982).
[33]W. F. Krupke, M. D. Shinn, J. E. Marion, J. A. Caird, and S. E. Stokowski, J. Opt. Soc. Am. B **3**, 102 (1986).
[34]M. D. Shinn, F. P. Milanovich, and J. N. Roe (unpublished).
[35]Y. Guyot, H. Manaa, R. Moncorgé, N. Garnier, E. Descroix, and P. Laporte, J. Phys. (Paris) Colloq. **4**, C4-529 (1994).
[36]U. Oeliker, M. J. Riley, P. S. May, and H. U. Gudel, J. Lumin. **53**, 553 (1992).
[37]J. Mares, B. Jacquier, P. Pédrini, and G. Boulon, Mater. Chem. Phys. J **21**, 237 (1989).
[38]G. E. Venikouas, G. J. Quarles, J. P. King, and R. C. Powell, Phys. Rev. B **30**, 2401 (1984); G. J. Quarles, G. E. Venikouas, and R. C. Powell, Phys. Rev. B **31**, 6935 (1985).
[39]M. A. Kramer and R. W. Boyd, Phys. Rev. B **23**, 986 (1981).
[40]T. Y. Fan and R. L. Byer, J. Opt. Soc. Am. B **11**, 1519 (1986).
[41]J. H. Schloss, L. L. Chase, and L. K. Smith, J. Lumin. **48-49**, 857 (1991).
[42]R. Buisson, J. Q. Liu, and J. C. Vial, J. Phys. **45**, 1533 (1984).
[43]R. B. Barthem, R. Buisson, J. C. Vial, and H. Harmand, J. Lumin. **34**, 295 (1986).
[44]T. Chuang and H. Verdun, in *Advanced Solid State Lasers Technical Digest, 1994* (Optical Society of America, Washington, D.C., 1994), p. 239.
[45]F. Auzel, J. Lumin. **31-32**, 759 (1984).
[46]W. Seelert, H. P. Lortz, and W. M. Yen, in *OSA Proceedings on Advanced Solid State Lasers,* edited by L. L. Chase and A. Pinto (Optical Society of America, Washington, D.C., 1992), Vol. 13, p. 209.
[47]Y. Guyot, Doctoral thesis, University of Lyon I, 1993.